Astron. Astrophys. 331, 829–837 (1998)

ASTRONOMY AND ASTROPHYSICS

The skewness and kurtosis of the projected density distribution function: validity of perturbation theory

E. Gaztañaga[1,2] **and F. Bernardeau**[3]

[1] Institut d'Estudis Espacials de Catalunya, Unidad Nixta del CSIC, Edf. Nexus-104 - c/ Gran Capitan 2-4, E-08034 Barcelona, Spain
[2] NASA/Fermilab Astrophysics Center, Fermilab, Batavia, IL 60510, USA
[3] Service de Physique Théorique, C.E. de Saclay, F-91191 Gif-sur-Yvette cedex, France

Received 17 July 1997 / Accepted 10 November 1997

Abstract. We study the domain of validity of Perturbation Theory (PT), by comparing its predictions for the reduced skewness, s_3, and kurtosis, s_4, of the projected cosmological density field, with the results of N-body simulations. We investigate models with different linear power spectra and consider as physical applications both angular galaxy catalogues and weak lensing surveys. We first find that the small-angle approximation for the predicted skewness provides a good match to the exact numerical PT results. On the other hand, results from non-linear simulated catalogues agree well with PT results on quasi-linear angular scales, which correspond to scales larger than about $1\,deg$ in the applications we have considered. We also point out that projection effects tend to attenuate the effects of strong non-linearities in the angular skewness and kurtosis.

Key words: cosmic microwave background – dark matter – gravitational lensing – large-scale structure of Universe

1. Introduction

One of the principal goal of the large galaxy surveys that should be available in the near future (SDSS, 2DF, MEGACAM project, ...) is the accurate determination of the power spectrum of density fluctuations, $P(k)$. Its interpretation in terms of cosmological models, however, requires an understanding of the way galaxies trace the underlying matter distribution. This is a general problem that is bound to become even more crucial with these new observational data.

It has been stressed recently (Fry & Gaztañaga 1993, Gaztañaga & Frieman 1994, Fry 1996, Bernardeau 1995, hereafter B95) that one way to address this problem is to consider higher-order correlation functions or higher-order moments of the local density probability distribution function. This approach is particularly attractive because, in the case of Gaussian initial conditions, Perturbation Theory (PT) provides precise quantitative predictions. It has now been well established that the p-order cumulants of the local density field $\left\langle \delta^p \right\rangle_c$ are expected to behave as

$$\left\langle \delta^p \right\rangle_c = S_p \left\langle \delta^2 \right\rangle^{p-2} \tag{1}$$

on large scales (Fry 1984, Goroff et al. 1986, Bouchet et al. 1992, Bernardeau 1992). The S_p parameters, which quantify the departure from Gaussian behavior, depend however on the window function applied to the field. In Bernardeau (1994) a prescription is given for the PT calculation of all these coefficients for a 3D top hat window function. These results have been subsequently checked in detail and found to be very accurate when compared to numerical simulations (Baugh et al. 1995, Gaztañaga & Baugh 1995). Perturbation results for the 3D Gaussian window function (Goroff et al. 1986, Juszkiewicz et al. 1993) for S_3 and S_4 have also been successfully tested against numerical simulations. Another fruitful direction of investigation is the calculation of the high-order correlation functions for the projected density (B95). This is an interesting domain of investigation since angular galaxy catalogs contain more objects and volume than 3D catalogs and therefore allow the determination of many more parameters of the hierarchy (1).

There is also a new mean of investigation, which is still in an embryonic state but might reveal extremely fruitful, for the projected density. The measurement of the gravitational weak shear induced by the large scale structures in deep galaxy catalogs allow in principle to have access to the correlation properties of the projected mass. The resulting polarization maps could allow the determination of these correlation functions at the level of the two-point function (Blandford et al.1991, Miralda-Escudé 1991, Villumsen 1996, Jain & Seljak 1997, Kaiser 1997) or even for higher orders (Bernardeau et al. 1997).

Although the projected density is obtained with completely different methods in galaxy catalogs or in weak lensing surveys, the properties of the projected density as yielded by Perturbation Theory are addressed in very similar ways. These two cases differ only in the shape of the required selection function,

Send offprint requests to: F. Bernardeau (fbernardeau@cea.fr)

whereas identical approximations are made in the course of the calculations for the derivation of the analytic expressions. We recall here that Perturbation Theory results are valid at large scales, where the variance is small. For 3D filtering, investigations in numerical simulations have proved that PT results are valid for scales above about $10\,h^{-1}$Mpc, where the variance of fluctuations approaches unity. In the case of the projected density, however, a given angular scale cannot be straightforwardly associated with a physical scale, since it corresponds to a superposition of different scales. A priori it is therefore difficult to assess the validity domain of PT results, even in light of the 3D cases. Another concern is the use of the small angle approximation. This is a mathematical approximation that allows one to dramatically simplify the calculations. So far it has not been possible to get closed analytic formulae without its use. This approximation might be not fully valid when the smoothing angle is above 1 degree (see B95).

The aim of this paper is therefore to investigate the validity of both the small angle and the PT approximations. Numerical simulations with N-body codes are used to check the validity of PT at small scales, and to give better clues to the importance of the fully non-linear corrections that may affect the quantities we are interested in. The effect of the small-angle approximation is more particularly investigated by direct Monte-Carlo integration of the s_3 coefficient. In this case, the problem is not the validity of the Perturbation Theory approach, but the accuracy of the mathematical approximations that were made in the course of the calculation.

In Sect. 2, we specify the models that are used to illustrate those calculations. We also give the expected values for s_3 in those cases. In Sect. 3 and Sect. 4, we confront those predictions with the Monte-Carlo calculations and the simulations.

2. The physical models

To illustrate our calculations we consider two different cases for the linear density power spectrum. We also consider two different physical applications: the selection function corresponding to angular catalogs and that corresponding to detection of weak shear.

2.1. The power spectra

In our first investigation we use the power spectrum derived from the angular APM Galaxy Survey (Maddox et al. 1990), which has been found to be well described by (Baugh & Gaztañaga, 1996)

$$P_{APM}(k) \propto \frac{k}{\left[1+(k/k_c)^2\right]^{3/2}}, \tag{2}$$

with

$$k_c \approx 150\ H_0/c. \tag{3}$$

In the second case, we use the standard CDM model with $\Omega_{\rm baryon} = 0.05$, $H_0 = 50\ km/s/$Mpc $\Omega_0 = 1$, $\Lambda = 0$, and an initial Harrison-Zel'dovich spectrum. For convenience the mass fluctuation power spectrum is approximated by a simple analytic fit (similar to the ones proposed by Bond & Efstathiou 1984),

$$P_{CDM}(k) = A\,\frac{k}{\left(1+\left[a\,k+(b\,k)^{3/2}+(c\,k)^2\right]^u\right)^{2/u}}, \tag{4}$$

with $u = 1.13$, $a = \dfrac{6.5}{3000\,\Gamma}$, $b = \dfrac{3}{3000\,\Gamma}$ $c = \dfrac{1.7}{3000\,\Gamma}$ $\Gamma = 0.5$, where the dimensional quantities have been expressed in such a way that $c = H_0 = 1$.

2.2. The angular galaxy catalogue selection function

In this case the local projected density field ω in the direction γ is given by

$$\delta_\gamma = \int {\rm d}r\ r^2\ F(r)\ \delta(r,\gamma), \tag{5}$$

where $\delta(r,\gamma)$ is the local over-density in the direction γ at the distance r, and $F(r)$ is the *normalized* selection function for the catalogue,

$$\int {\rm d}r\ r^2\ F(r) = 1. \tag{6}$$

In case of the APM angular survey the radial selection function is given in Gaztañaga (1995), Gaztañaga & Baugh (1997, hereafter GB97). This function can be approximated by:

$$F(r) \propto r^{-b}\ \exp[-r^2/D^2]. \tag{7}$$

We will use $b \simeq 0.1$ and $D \simeq 335h^{-1}$Mpc, which provides a good fit to the APM selection function, as shown in Fig. 1 (see §4, below).

We can calculate the moments of the distribution of the local projected density δ_θ, smoothed at scale θ (see Bernardeau 1995, Pollo & Juszkiewicz 1997) using Perturbation Theory and the small angle approximation. These moments can be writen in terms of:

$$\left\langle \delta_\theta^2 \right\rangle = \frac{1}{V_{\rm cone}^2} \int\int_{V_{\rm cone}} d^3\mathbf{r}_1\ {\rm d}^3\mathbf{r}_2\ \xi_2(\mathbf{r}_1,\mathbf{r}_2), \tag{8}$$

$$\left\langle \delta_\theta^3 \right\rangle = \frac{1}{V_{\rm cone}^3} \int\int\int_{V_{\rm cone}} {\rm d}^3\mathbf{r}_1\ {\rm d}^3\mathbf{r}_2\ {\rm d}^3\mathbf{r}_3\ \xi_3(\mathbf{r}_1,\mathbf{r}_2,\mathbf{r}_3), \tag{9}$$

where ξ_2 and ξ_3 are respectively the two and three-point correlation functions in real space and $V_{\rm cone}$ is the 'volume' of the cone of angle θ and a radial distribution given by the selection function $F(r)$. The second moment, or variance of angular counts-in-cells, at the smoothing scale θ, defined in (8), can also be given by

$$\left\langle \delta_\theta^2 \right\rangle = \frac{1}{2\pi} \int {\rm d}r\ r^4\ F^2(r) \int k\,{\rm d}k\ P(k)\ W_{2D}(k\,\theta) \tag{10}$$

where W is the window function in k space. This variance can also be related to an area average over the two-point angular

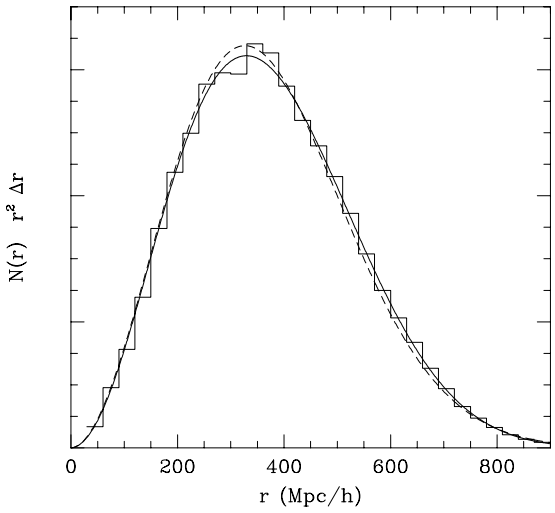

Fig. 1. Comparison the theoretical (lines) and measured counts (histogram) in radial shells for a mock catalogues. The dashed line is a model while the continuous line corresponds to the input APM selection function.

correlation (e.g. Gaztañaga 1994, hereafter G94). Note that this expression does not rely on perturbative calculation if the power spectrum that is used is the final one. It uses, however the small angle approximation. In the following we will use exclusively the top-hat window function so that

$$W_{2D}(k\theta) = 2\ \frac{J_1(k\theta)}{k\theta}, \tag{11}$$

where J_1 is the spherical Bessel Function. The third moment of smoothed angular fluctuations, defined in (9), is given by

$$\left\langle \delta_\theta^3 \right\rangle = \frac{6}{(2\pi)^2} \int dr\ r^6 F^3(r) \left[\frac{6}{7} \left(\int k\mathrm{d}k W_{2D}^2(k\,\theta)\, P(k) \right)^2 \right.$$
$$+ \frac{1}{2} \int k\,\mathrm{d}k\, W_{2D}^2(k\,\theta)\, P(k) \times \tag{12}$$
$$\left. \int \frac{k\,\mathrm{d}k}{\theta}\, W_{2D}(k\,\theta)\, W'_{2D}(k\,\theta)\, P(k) \right]$$

were W'_{2D} is the derivative of W_{2D}. So that, in case of a power law spectrum $P(k) \sim k^n$, we have (B95),

$$s_3^{\mathrm{Gal.}} \equiv \frac{\left\langle \delta_\theta^3 \right\rangle}{\left\langle \delta_\theta^2 \right\rangle^2} = R_3\ \left(\frac{36}{7} - \frac{3}{2}\,(n+2) \right), \tag{13}$$

with

$$R_3 = \frac{\int r^{8-2(n+3)}\ \mathrm{d}r\ F^3(r)}{\left[\int r^{5-(n+3)}\ \mathrm{d}r\ F^2(r) \right]^2}, \tag{14}$$

for a normalized selection function. The coefficient R_3 is found in practice to be of order unity and to be very weakly dependent on the adopted shape for the selection function. Note however that the redshift evolution of the fluctuations has not been taken into account in this relation. This evolution should be taken into account for catalogs having a large depth. In this case, the geometrical factors for non-flat universes are also important (see G94).

For the selection function given in Eq. (7) we can calculate $s_3^{\mathrm{Gal.}}$ explicitly,

$$s_3^{\mathrm{Gal.}} = \frac{8}{3\sqrt{3}} \left(\frac{\sqrt{27}}{4} \right)^b \frac{\Gamma[3/2 - b/2]\Gamma[3/2 - n - 3/2\ b]}{\Gamma[3/2 - n/2 - b]^2}$$
$$\times \left(\frac{3}{2} \right)^n \left[\frac{36}{7} - \frac{3}{2}(n+2) \right]. \tag{15}$$

For $b = 0$ and $n = 0$ we find $R_3 = \frac{8}{3\sqrt{3}} \simeq 1.54$, while for $b = 0$ and $n = -1$, closer to the APM case, $R_3 = \frac{2\pi}{3\sqrt{3}} \simeq 1.21$, comparable to the values given in G94.

2.3. The weak lensing efficiency function

In the case of weak lensing the local projected density cannot be directly observed. We can however observe the local convergence (see Kaiser 1995, Bernardeau et al. 1997) κ,

$$\kappa(\gamma) = -\frac{3}{2}\,\Omega_0 \int \mathrm{d}r\ E(r)\ \delta(r,\gamma) \tag{16}$$

where the efficiency function, $E(r)$, depends on the redshift distribution of the lenses. For simplicity we assume that the lenses are all at redshift $z = 1$ and that we live in an Einstein-de Sitter Universe. In this case we have

$$E(r) = \frac{r\,(r_s - r)}{r_s}\ \left(\frac{2}{2 - r} \right)^2, \tag{17}$$

with

$$r_s = 2 - \sqrt{2}. \tag{18}$$

Here the second and third moment are given by

$$\left\langle \kappa^2(\theta) \right\rangle = \frac{3}{4\pi}\ \int \mathrm{d}r\ E^2(r) \int k\,\mathrm{d}k\ P(k)\ W_{2D}(k\,\theta) \tag{19}$$

and

$$\left\langle \kappa^3(\theta) \right\rangle = \tag{20}$$
$$-\frac{27}{2\,(2\pi)^2} \int_0^{r_s} \mathrm{d}r\ E^3(r) \left[\frac{6}{7} \left[\int k\mathrm{d}k W_{2D}^2(k\,\theta)\, P(k) \right]^2 \right.$$
$$+ \frac{1}{2} \int k\,\mathrm{d}k\, W_{2D}^2(k\,\theta)\, P(k) \times$$
$$\left. \int \frac{k\,\mathrm{d}k}{\theta}\, W_{2D}(k\,\theta)\, W'_{2D}(k\,\theta)\, P(k) \right]$$

These moments can be calculated explicitly only for particular power spectra. In the case of a power law spectrum of index

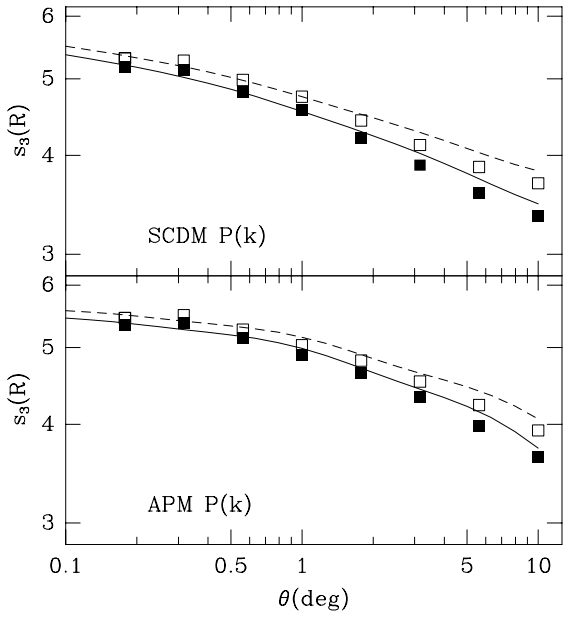

Fig. 2. Angular skewness s_3 for galaxy catalogue selection function from Monte-Carlo integration (symbols) compared with small angle approximation PT predictions (lines). The open symbols and dashed line include (linear) redshift evolution.

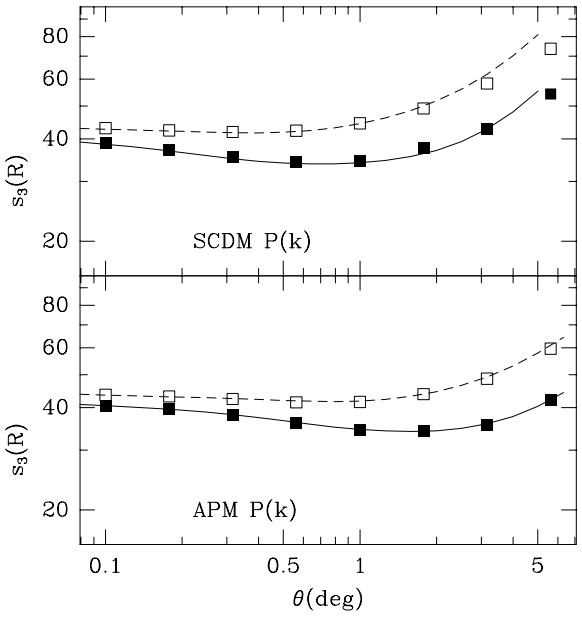

Fig. 3. Angular skewness s_3 for weak lensing efficiency function from Monte-Carlo integration (symbols) compared with small angle approximation PT predictions (lines). The opened symbols and dashed line include (linear) redshift evolution.

n, we have (see Bernardeau et al. 1997),

$$s_3^{\rm WL} = -\left[\frac{36}{7}-\frac{3}{2}(n+2)\right](n-1)(n-2)(n-3)^2\times \left[40-2\,n\,(2\,n-1)-\frac{32\,n}{\sqrt{2}}\right]/ \left[16\,n\,(2\,n-5)\,(2\,n-3)\,(2\,n-1)\,\left(2-\sqrt{2}\right)^2\right]. \quad (21)$$

In the following we will compare these P.T. results with results of numerical simulations.

3. A Monte-Carlo integration for s_3

The aim of these Monte-Carlo integrations is to check the validity of the small angle approximation in PT. The integration is made here in real space by throwing points at random in conical cells and by calculating the averages of the second and third correlation functions. We then identify the moments with the geometrical averages given by (8) and (9) over the the two and three-point correlation functions in real space. In Perturbation Theory they can both be expressed in term of the linear power spectrum,

$$\xi_2(\mathbf{r}_1,\mathbf{r}_2) = \int \frac{{\rm d}^3\mathbf{k}}{(2\pi)^3}\,P(k)\,\exp[{\rm i}\mathbf{k}\cdot(\mathbf{r}_2-\mathbf{r}_1)] = \int \frac{k^2\,{\rm d}k}{2\pi^2}\,P(k)\,\frac{\sin(k\,|\mathbf{r}_2-\mathbf{r}_1|)}{k\,|\mathbf{r}_2-\mathbf{r}_1|}, \quad (22)$$

and

$$\xi_3(\mathbf{r}_1,\mathbf{r}_2,\mathbf{r}_3) = \int \frac{{\rm d}^3\mathbf{k}_1}{(2\pi)^3}\,\frac{{\rm d}^3\mathbf{k}_2}{(2\pi)^3} \times P(k_1)\,\exp[{\rm i}\mathbf{k}_1\cdot(\mathbf{r}_2-\mathbf{r}_1)]\,P(k_2)\,\exp[{\rm i}\mathbf{k}_2\cdot(\mathbf{r}_3-\mathbf{r}_1)] \times \left[\frac{10}{7}+\frac{\mathbf{k}_1\cdot\mathbf{k}_2}{k_1^2}+\frac{\mathbf{k}_1\cdot\mathbf{k}_2}{k_2^2}+\frac{4}{7}\frac{(\mathbf{k}_1\cdot\mathbf{k}_2)^2}{k_1^2\,k_2^2}\right]+{\rm cyc.} \quad (23)$$

As shown in the appendix it is actually more convenient to express these quantities through a set of real space functions. Indeed, we can define the function $\varphi(r)$ by,

$$\varphi(r) = \int \frac{k^2\,{\rm d}k}{2\pi^2}\,\frac{P(k)}{k^2}\,\frac{\sin(k\,r)}{k\,r} \quad (24)$$

from the derivative of which the three point function can be expressed. The Monte-Carlo integrations can then be done in real space. They reduce to 6 dimensional integrals (see appendix) which can be done on common work stations.

In Fig. 2 and 3, we compare the results of the Monte-Carlo integration (symbols) for s_3 with the small angle approximation (curves) in PT. We show both the case with (linear) redshift evolution (open symbols and dashed line), which would correspond to real observations, and also the case without redshift evolution, as corresponds to the comoving output from N-body simulations (see below).

There is an excellent agreement in the comparison specially in the weak lensing case. For the galaxy selection function there are some small discrepancies at the largest scales, but they are smaller than the typical errors in the estimation from the observations. Thus the small angle approximation seems to be quite good for most applications up to 10 degree scales.

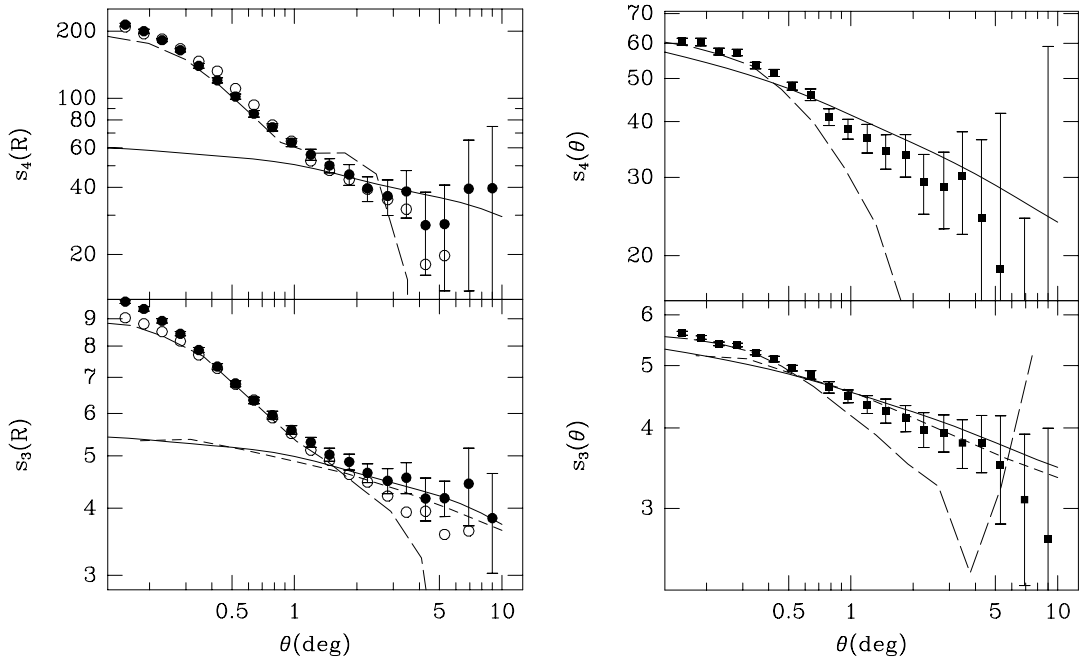

Fig. 4. Angular skewness s_3 (bottom) and kurtosis s_4 (top) in mock maps with the APM power spectrum (left panels) and the CDM power spectrum (right panels) for the galaxy catalogue selection function. Results are symbols with errorbars and are compared with small angle approximation PT predictions (continuous line). The short-dashed line shows the Monte Carlo integration. The long-dashed line are results from smaller mock catalogues with the (APM) observational mask.

Table 1. Simulation parameters

run	number of particles	mesh	L_{box} (h^{-1}Mpc)
APM1 (a)-(e)	126^3	128^3	400
APM2 (a)-(b)	200^3	128^3	600
CDM (a)-(e)	126^3	128^3	378

4. The numerical N-body results

We study two shapes of the power spectrum: the APM model and the CDM model, as described in Sect. 2. We use several sets of N-body simulations with parameters shown in Table 1. The letters refer to different realizations of each model: 5 for APM1, 2 for APM2 and 5 for CDM. The APM like models are described in detail in GB97, while the CDM simulations are from GB95, and correspond to the standard model: $\Gamma = 0.5$.

For the APM like models we use the output time corresponding to the measured APM amplitude, $\sigma_8 \simeq 0.8$ (note that this value does not take into account any evolution in the clustering, and corresponds to clustering at the mean redshift in the APM, e.g. G95, $\simeq 400h^{-1}$Mpc). For CDM models we use $\sigma_8 = 1$, unless otherwise stated. As we are using outputs in comoving coordinates, there is no redshift evolution within one output. This is not the case in the real Universe, but we take this into accunt in the theoretical predictions in a straightforward way (G94, see Fig. 2 and 3).

To produce the angular catalogues we first select an arbitrary point in the simulated box to be the local 'observer'. We include a simulated particle at comoving coordinate r from the observer with probability given by the selection function $F(r)$, in the case of galaxy clustering, or the efficiency function in the case of weak lensing, as described in Sect. 2. As the simulation is done in a periodic box, we replicate the box to cover the total radial extent of the APM. Although the depth is only $\simeq 400h^{-1}$Mpc, the mean number of galaxies drops quickly thereafter and the expected number of galaxies is larger than unity up to a radial distance of $1200h^{-1}$Mpc. The main difference with GB97, is that they apply the APM angular survey mask, including plate shapes and holes, whereas here we use full sky maps, which cover a larger area and have no boundaries. In our full sky mock catalogues there could be a certain degree of repetition and correlations between the boxes, but the errors are estimated form the dispersion in different catalogues. By comparing the results from different box sizes we have verified that this replication of the box does not introduce any spurious effects (see below). The total number of particles in the mock angular catalogues is about 9×10^6 for the APM galaxy selection function and about 25×10^6 for the weak lensing case.

Fig. 1 shows a comparison between the expected number of galaxies, $N(r)r^2\Delta r$, at different radial depths (in comoving coordinates r) given by the input selection function, as compared to the measured counts in a mock catalogue. The dashed line is

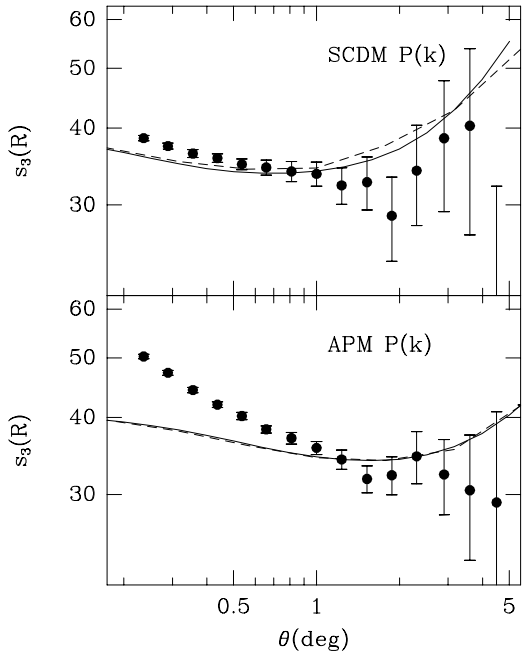

Fig. 5. Angular skewness s_3 for weak lensing efficiency function from simulations compared with small angle approximation PT predictions (continuous line). The short-dashed line shows the Monte Carlo integration.

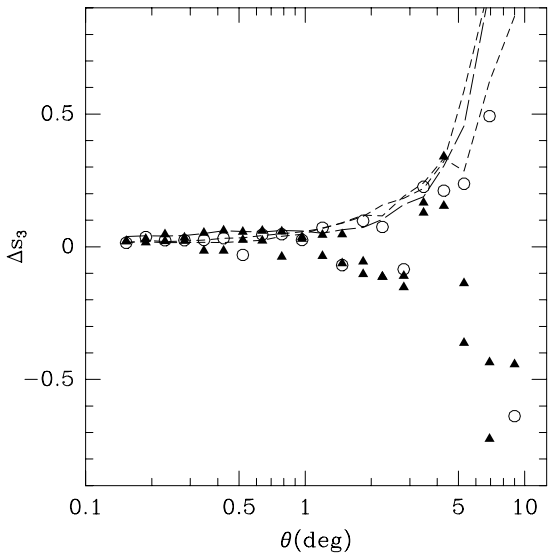

Fig. 6. Relative errors in the the distribution of values of $s3$ from different maps as a function of the angular scale. Dashed line corresponds to the rms value: $\left\langle (\Delta s_3)^2 \right\rangle^{1/2}$, whereas the points correspond to a measure of the skewness: $\left\langle (\Delta s_3)^3 \right\rangle^{1/3}$. Open circles and long dashed lines correspond to the maps from the largest box simulations. Filled triangles and short-dashed lines show resulsts from the small boxes.

the model in Eq. (7) for $b \simeq 0.1$ and $D \simeq 335h^{-1}$Mpc, while the continuous line is the input APM selection function (GB97).

From each realization we produce several mock catalogues by choosing different positions for the observer. Because of the selection function, catalogues from different observers are not necessarily correlated. Three different observers are used for the smaller boxes. For the larger boxes the corresponding number is 10 observers. For these numbers, results from different observers do not seem to be correlated. Thus the total number of mock catalogues is 15 for APM1 and CDM, and 20 for APM2.

Fig. 4 shows the results for s_3 and s_4 for the galaxy CDM and APM2 mock catalogues. Results for APM1 catalogues, which are shown as open symbols in the figure, agree well with the ones in APM2, indicating that the size of the simulation box, which is changed by over a factor of 3 in this comparison, is large enough and that the box replication is not an important effect. We have also performed a similar test with $180h^{-1}$Mpc boxes, Ensemble A in Baugh et al. 1995, probing over a factor of 10 in volume.

There is very good agreement between the N-body results and PT theory at scales $\theta \gtrsim 2\,deg$ for the APM model. For CDM, there is agreement within the errors for $\theta \gtrsim 1\,deg$, although this is not as good as for the APM model. This could be due to finite volume effects, which seem more important for CDM (see below); note also that the CDM errors are larger and that the CDM maps come from a simulation with a smaller volume. Scales $\theta \simeq 1\,deg$ in the CDM models could also be affected by projection effects that tend to overcompensate non-linearities (see below); this is more important for CDM which has a higher normalization (σ_8 = 1).

Fig. 5 shows a comparison of PT with the skewness estimated in the mock maps made with the weak lensing efficiency function. The errors are larger here than in the galaxy case because the depth (and volume) is larger and therefore a given physical scale corresponds to a smaller angular scale.

4.1. Sampling variance

We find that it is crucial to use a large number of catalogues in order to have a robust estimation at the largest angular scales. This is illustrated in Fig. 6, which shows moments of the distribution of relative errors in s_3, i.e. $\Delta s_3 \equiv s_3/\bar{s}_3 - 1.$, from map to map around the mean value, $\bar{s}_3$. The rms error (dashed line) increases with angular scale as expected. The skewness of the error distribution, $\left\langle (\Delta s_3)^3 \right\rangle^{1/3}$ (points in the figure), has large fluctuations, but seems to have a tendency to go negative on the largest scales in each catalogue. We show results for both the large APM simulations (open circles and long dashed lines) and both CDM and APM L = $400h^{-1}$Mpc simulations. This result indicates that it is more likely to find smaller values of s_3, when doing a smaller sampling, e.g. in a single map.

The above arguments are also illustrated by comparing the results from the full sky mock catalogues with the mean values using 10 mock catalogues with the APM mask (e.g. GB97). The latter not only cover a smaller fraction of the sky (only about 10%) but are also subject to boundary effects. The results for these *realistic* maps are shown as long-dashed lines in Fig. 4.

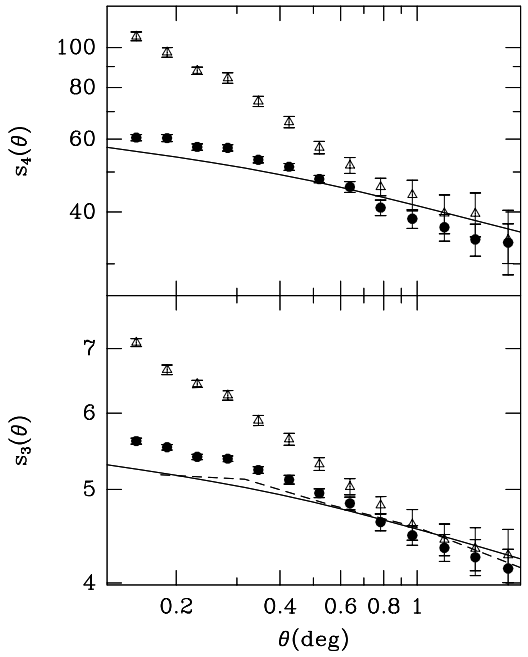

Fig. 7. Angular skewness (bottom) and kurtosis (top) in CDM mock maps from different output times: $\sigma_8 = 1$ (filled circles) and $\sigma_8 = 0.5$ (open triangles). Continuous lines show the small angle approximation PT predictions. The short-dashed line shows the Monte Carlo integration.

The finite volume and boundary effects seem important on scales $\theta \gtrsim 1\, deg$ for CDM and about $\theta \gtrsim 2\, deg$ for APM.

4.2. Time evolution

Perturbation theory predicts time independent values of the skewness, in the limit of small variance. For large variance, N-body simulations find that the 3D skewness, S_3, increases with time due to non-linear effects (e.g. Baugh et al. 1995, Colombi et al. 1997). Non-linearities also erase the shape dependence in the hierarchical structure, e.g. the bispectrum, (see Scoccimarro et al. 1997) reproducing a simple tree-level hierarchy, independent of the shape of the configurations. When this happens there is a simple relation between the angular and 3D skewness: $s_3 \simeq R_3\, S_3$ (see G94), so that the corresponding 2D projected amplitudes are closer to the 3D PT results. Thus, on quasi-linear scales, the relation $s_3 \simeq R_3\, S_3$ typically underestimates the projection effects, while it should be more accurate on smaller scales, were PT results will overpredict the projection effect.

Fig. 7 shows a comparison of s_3 and s_4 from mock maps drawn from two different outputs in the CDM galaxy model. Contrary to what one would expect, the later output seems closer to PT results. This is because of the projection effects mentioned above, which compete with the non-linear growth in s_3. In fact, the slight disagreement at the smallest angular scales between the results of the full sky map (symbols with errorbars) and the one with the APM mask (long-dashed lines) shown in Fig. 4 is also due to the fact that we have used slightly different output times in each case.

5. Conclusion

We conclude from this analysis that the P.T. results for the skewness and kurtosis are accurate at degree scales or larger for the projected density. Comparisons between Monte-Carlo integrations and results obtained from the small-angle approximation are in good agreement. A departure starts to be noticeable only for smoothing scales above 5 degrees, but even there it is small compared with typical errors.

The N-body results allow us to estimate the small angular scales at which nonlinear effects start to affect the values of s_3. We found these effects to be important below $0.5\, deg$ for the lensing case, and below $1\, deg$ for the galaxy selection function, with a rapid growth of s_3 at small scale. This however depends strongly on the initial power spectrum. This effect is found to be more important for the measured APM power spectrum than for the CDM one.

We have found two effects that might prove important in comparing perturbation theory with observations of angular clustering, and in particular for the APM. First, volume and boundary effects are important on scales $\gtrsim 2$ deg and tend to produce smaller values of s_3 and s_4. We argue that this is not because the mean is biased, but because the distribution of errors seems to be negatively skewed (e.g. Fig. 6) and it is therefore more probable to find smaller values. Second, the tree-level hierarchy model for projections commonly used in the literature (e.g. by Groth & Peebles 1977, Fry & Peebles 1978, Peebles 1980, Szapudi et al. 1992, Szapudi et al. 1995), and in particular for the APM (G94) is not accurate on quasi-linear scales, as indicated in B95, because it underestimates the projection factors. At small scales, non-linear effects tend to mix these two cases (e.g. Fig. 7), while at larger scales this competes with large volume effects. The errors involved are of the order of 20% in s_3, but more quantitative analysis of this point and implications for the APM observations will be presented elsewhere.

To have a better insight into these nonlinear effects, and how it depends on the shape of the power spectrum, it could be fruitful to extend the recent results of Scoccimarro (1997) on the one-loop correction of the bispectrum to the projected third moment.

Acknowledgements. We would like to thank Fermilab group for their kind hospitality during our visit in the fall 1996. EG would like to thank Carlton Baugh and Josh Frieman for help and comments on the manuscript. E.G. acknowledges support from CIRIT (Generalitat de Catalunya) grant 1996BEAI300192, CSIC, DGICYT (Spain), project PB93-0035, and CIRIT, grant GR94-8001.

Appendix: the expression of the three-point correlation function in real space

We want to express the three point correlation function provided by Perturbation Theory (Peebles 1980, Fry 1984),

$$\xi_3(\mathbf{r}_1,\mathbf{r}_2,\mathbf{r}_3) = \int \frac{\mathrm{d}^3\mathbf{k}_1}{(2\pi)^3}\,\frac{\mathrm{d}^3\mathbf{k}_1}{(2\pi)^3} \tag{A1}$$
$$\times\, P(k_1)\,\exp[\mathrm{i}\mathbf{k}_1\cdot(\mathbf{r}_2-\mathbf{r}_1)]\,P(k_2)\,\exp[\mathrm{i}\mathbf{k}_2\cdot(\mathbf{r}_3-\mathbf{r}_1)]$$
$$\times\,\left[\frac{10}{7}+\frac{\mathbf{k}_1\cdot\mathbf{k}_2}{k_1^2}+\frac{\mathbf{k}_1\cdot\mathbf{k}_2}{k_2^2}+\frac{4}{7}\frac{(\mathbf{k}_1\cdot\mathbf{k}_2)^2}{k_1^2\,k_2^2}\right]+\text{cyc.}$$

in real space only. The reason is that the integration in k space with real space top-hat window function is hardly possible because the integrals converge very slowly.

Let us introduce the function $\varphi(r)$,

$$\varphi(r) \;=\; \int \frac{\mathrm{d}^3\mathbf{k}}{(2\pi)^3}\,\frac{P(k)}{k^2}\,\exp(\mathrm{i}\mathbf{k}\cdot\mathbf{x}) \tag{A2}$$
$$\;=\; \int \frac{k^2\,\mathrm{d}k}{2\pi^2}\,\frac{P(k)}{k^2}\,\frac{\sin(k\,r)}{k\,r}. \tag{A3}$$

Then we can notice that

$$\nabla\xi(\mathbf{x}) \;=\; -\mathrm{i}\int \frac{\mathrm{d}^3\mathbf{k}}{(2\pi)^3}\,\mathbf{k}\,\exp(\mathrm{i}\mathbf{k}\cdot\mathbf{x}) \tag{A4}$$
$$\;=\; \frac{\mathbf{x}}{x}\,\frac{\mathrm{d}\xi(x)}{\mathrm{d}x} \tag{A5}$$

(and a similar property for φ) so that

$$\nabla\xi(\mathbf{x}_{12})\cdot\nabla\varphi(\mathbf{x}_{13}) \tag{A6}$$
$$= -\int \frac{\mathrm{d}^3\mathbf{k}_1}{(2\pi)^3}\,\frac{\mathrm{d}^3\mathbf{k}_2}{(2\pi)^3}\,\frac{\mathbf{k}_1\cdot\mathbf{k}_2}{k_2^2}\,\exp(\mathrm{i}\mathbf{k}_1\cdot\mathbf{x}_{12}+\mathrm{i}\mathbf{k}_2\mathbf{x}_{13})$$
$$= \frac{\mathbf{x}_1 2\cdot\mathbf{x}_{13}}{x_{12}x_{13}}\,\frac{\mathrm{d}\xi(x_{12})}{\mathrm{d}x_{12}}\,\frac{\mathrm{d}\varphi(x_{13})}{\mathrm{d}x_{13}} \tag{A7}$$

and one recognizes one term that intervenes in the expression of the three-point function.

To complete the calculation one can also notice that,

$$\varphi_{ij}(\mathbf{x}_{12})\varphi_{ij}(\mathbf{x}_{13}) \tag{A8}$$
$$= \int \frac{\mathrm{d}^3\mathbf{k}_1}{(2\pi)^3}\,\frac{\mathrm{d}^3\mathbf{k}_2}{(2\pi)^3}\,\frac{(\mathbf{k}_1\cdot\mathbf{k}_2)^2}{k_1^2\,k_2^2}\,\exp(\mathrm{i}\mathbf{k}_1\cdot\mathbf{x}_{12}+\mathrm{i}\mathbf{k}_2\mathbf{x}_{13})$$
$$= \frac{\varphi'(x_{12})\,\varphi'(x_{12})}{x_{12}\,x_{13}}+\varphi''(x_{12})\,\varphi''(x_{13})+$$
$$\frac{(\mathbf{x}_{12}\cdot\mathbf{x}_{13})^2}{x_{12}\,x_{13}}\,\left(\varphi''(x_{12})-\frac{\varphi'(x_{12})}{x_{12}}\right)\,\left(\varphi''(x_{13})-\frac{\varphi'(x_{13})}{x_{13}}\right).$$

Finally remarking that

$$\varphi''(x) = -\xi_2(x) - \frac{2}{x}\varphi'(x) \tag{A9}$$

one can express the three point correlation function in real space with the function $\xi_2(x)$, $\xi_2'(x)$ and $\varphi'(x)$ only:

$$\xi_3(\mathbf{r}_1,\mathbf{r}_2,\mathbf{r}_3) = \frac{10}{7}\xi_2(x_{12})\,\xi_2(x_{13})+$$

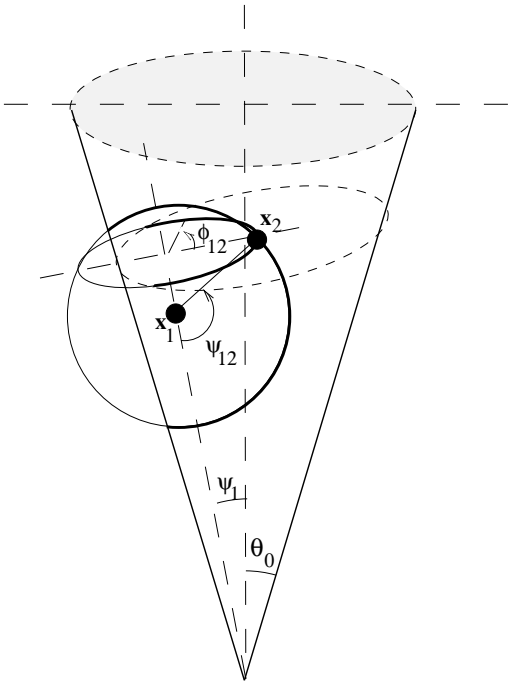

Fig. 8. Description of the variables used in the Monte Carlo Integration. The distance of $\mathbf{x}_1$ to the origin, the distance between $\mathbf{x}_1$ and $\mathbf{x}_2$, the angle Ψ_1 and the angle Ψ_{12} are all chosen randomly. The integration over ϕ_{12} can be done explicitly since the distances of $\mathbf{x}_2$ to the origin and to $\mathbf{x}_1$ remain then constant.

$$\frac{4}{7}\frac{\varphi'(x_{12})}{x_{12}}\,\frac{\varphi'(x_{13})}{x_{13}}+$$
$$\frac{4}{7}\,\left(\xi_2(x_{12})+2\frac{\varphi'(x_{12})}{x_{12}}\right)\,\left(\xi_2(x_{13})+2\frac{\varphi'(x_{13})}{x_{13}}\right)$$
$$-u\,\left[\xi_2'(x_{12})\,\varphi'(x_{13})+\xi_2'(x_{13})\,\varphi'(x_{12})\right]+ \tag{A10}$$
$$\frac{4}{7}\,u^2\,\left(\xi_2(x_{12})+3\frac{\varphi'(x_{12})}{x_{12}}\right)\,\left(\xi_2(x_{13})+3\frac{\varphi'(x_{13})}{x_{13}}\right)+\text{cyc.},$$

where

$$u \equiv \frac{\mathbf{x}_{12}\cdot\mathbf{x}_{13}}{x_{12}\,x_{13}}. \tag{A11}$$

This result generalizes the one obtained by Fry (1984) for power law spectra.

The Monte-Carlo computations of the geometrical averages of ξ_2 and ξ_3 can then be done in real space, provided the functions ξ_2, ξ_2' and φ' are known. Then the integrations can be reduced to a 6-dimensional integrals by direct integration over the azimuthal angles (see Fig. 3).

References

Baugh C.M., Gaztañaga E., 1996, MNRAS, 280, L37
Baugh C.M., Gaztañaga E., Efstathiou G., 1995, MNRAS, 274, 1049
Bernardeau F., 1992, ApJ, 392, 1
Bernardeau F., 1994 A&A 291, 697
Bernardeau F., 1995, A&A 301, 309. (B95)
Bernardeau F., van Waerbeke L., Mellier Y., 1997, A&A 322, 1

Blandford R. D., Saust A. B., Brainerd T. G., Villumsen J. V., 1991, MNRAS, 251, 600
Bond J. R., Efstathiou G., ApJ, 285L, 45
Bouchet F.R., Juszkiewicz R., Colombi S., Pellat R., 1992 ApJ, 394, L15
Colombi S., Bernardeau F., Bouchet F., Hernquist L., 1997 MNRAS, 287, 241
Fry J.N., 1984, ApJ, 279, 499
Fry J.N., 1996, ApJ, 469, L85
Fry J.N., Gaztañaga E., 1993, ApJ, 413, 447
Fry J.N., Peebles P.J.E., 1978, ApJ, 221, 19
Gaztañaga E., 1994, MNRAS, 268, 913 (G94)
Gaztañaga E., 1995, ApJ, 454, 561
Gaztañaga E., Baugh C.M., 1995, MNRAS, 273, L1.
Gaztañaga E., Baugh C.M., 1997, MNRAS, submitted, astro-ph/9704246 (GB97)
Gaztañaga E., Frieman J.A., 1994, Ap. J. (Letters), 425, 392
Goroff M.H., Grinstein B., Rey S.J., Wise M.B., 1986, ApJ, 311, 6
Groth E.J., Peebles P.J.E., 1977, ApJ, 217, 385
Jain B, Seljak U., 1997, ApJ, 484, 560
Juszkiewicz R., Bouchet F.R., Colombi S., 1993, ApJ, 412, L9
Kaiser N., 1995, ApJ, 439, 1
Kaiser N., 1997, ApJ, in press, astro-ph/9610120
Maddox S.J., Efstathiou G., Sutherland W.J., Loveday J., 1990, MNRAS, 242, 43p
Miralda-Escude J., 1991, ApJ, 380, 1
Peebles P.J.E., 1980, *The Large Scale Structure of the Universe:* Princeton University Press
Pollo A., Juszkiewicz R., 1997 in preparation
Scoccimarro R., Colombi S. et al., 1997, submitted to ApJ, , astro-ph/9704075
Scoccimarro R., 1997, submitted to ApJ, , astro-ph/9612207
Szapudi I., Szalay A.S., Boschan P., 1992, ApJ, 390, 350
Szapudi I., Dalton G.B., Efstathiou G., Szalay A.S, 1995, ApJ, 444, 520
Villumsen J., 1996, MNRAS, 281, 369

This article was processed by the author using Springer-Verlag LaTeX A&A style file *L-AA* version 3.